2026,Volume 3 , Issue 10 , PSIJK (80-93)

PURE SCIENCES International Journal of Kerbala

Pure Sciences International Journal of Kerbala

Rotational and MHD Effects on Pseudoplastic Nanofluid Peristaltic Transport in an Inclined Asymmetric Porous Channel

M. H. Ali [a*], M. R. Salman [b]

[a, b] *Department of Mathematics, College of Education for Pure Sciences, University of Karbala, Karbala, Iraq*

P A P E R I N F O

Received: 29 .03.2026
Accepted: 06.05.2026
Published: 30.06.2026

Keywords:
magnetohydrodynamic, Reynolds number, rotation, peristaltic transport, pseudoplastic nanofluid

A b s t r a c t

This study presents a mathematical model to study the peristaltic transport of a non-Newtonian pseudoplastic nanofluid in an asymmetric, inclined, rotating porous channel under magnetohydrodynamic (MHD) influences. The momentum, concentration, and energy equations are transformed into dimensionless, nonlinear ordinary differential equations by applying appropriate conversions. According to the assumptions of a long wavelength and low Reynolds number, approximate analytical solutions are obtained via the perturbation method, along with numerical solutions computed using MATHEMATICA. The effects of key physical parameters, including the Hartmann number, thermophoresis parameter, and rotation parameter, on the velocity distribution, temperature profile, nanoparticle volume fraction, and pressure rise are studied, as well as the trapping and pumping phenomena.

DOI: 10.53851/psijk.v3.i10. 80-93

Table 1. Nomenclature

NOMENCLATURE			
a	Amplitudes of lower walls	Ta	Taylor's Number
B_0	Magnetic parameter	T_m	Fluid mean temperature
b	Amplitudes of walls	T	Dimensionless time
Ω	Rotation parameter	$\acute{t}$	Dimensional time
D_B	Brownian diffusion coefficient	**Greek Symbols**	
D_T	thermophoretic diffusion coefficient	ρ_p	density of nano-particles
g	Acceleration	$\acute{\sigma}$	fluid electrical Conductivity
K_0	permeability parameter	σ^*	Stefan-Boltzmann constant
K	Darcy number	σ	Concentration
M	Hartman number	ρ_f	density of fluid
N_b	Brownian motion parameter	$\mathcal{K}$	Thermal conductivity of fluid
Nt	Thermophoresis parameter	Λ	Wavelength
Pr	Prandtl number	$\mathcal{T}$	Fluid temperature
$\tilde{P}$	Dimensional Pressure	Δ	wavenumber
p	Dimensionless pressure	$\mathcal{C}$	Nanoparticle concentration
Q_0	Constant heat addition/absorption	m	Dimensionless non-uniform parameter
Q	Dimensionless mean flows	$\mathcal{K}^*$	Mean absorption coefficient
Re	Reynolds number	A	Inclination of the channel with the horizontal
R_n	Thermal radiation parameter	θ	Dimensionless temperature
Sc	Schmidt number	M	fluid viscosity

*Corresponding Author Institutional Email:
ha80der@gamil.com (Hayder B. Abbas Al-Ghreaty)

1. Introduction

A kind of fluid movement known as peristaltic transport, takes place inside flexible tubes or small ducts. It is caused by periodic waves of contraction and relaxation in the duct walls, which push fluid in a specific direction without the need for external pressure. The moving passage of food from the oesophagus to the stomach, the flow of blood within microvasculature, and urine flow from the kidneys to the bladder all clearly illustrate this pattern of movement, making it a crucial topic in biomedical, industrial, and physiological research. The foundation for comprehending the phenomenon of peristaltic transport and its subsequent applications was laid by (Latham, 1966), who was the first to present a mathematical study describing the movement of fluid inside a flexible tube using a peristaltic wave. Jaffrin & Shapiro, (1969) explained the peristaltic mechanism within the system of the laboratory. There are currently numerous publications on peristalsis that consider various fluid models and flow configurations (Ali, 2021; Hasona et al., 2020; Hayat et al., 2017; Shapiro et al., 1969). The term "nano-fluid" was first used by (Choi, 1995) to refer to a fluid that contained nanoparticles with diameters typically under 50 nanometers. In particular, the inclusion of magnetic fields, porous media, and channel inclination has been shown to significantly influence flow and transport characteristics in non-Newtonian fluids. These effects are especially relevant in biomedical devices such as peristaltic micropumps, where peristalsis is employed to transport complex fluids, including blood and polymeric solutions. Consequently, an increasing number of studies have concentrated on examining peristaltic transport under various combinations of magnetohydrodynamic, porous, and geometrical effects. An investigation was conducted into how Soret and Dufour affected the peristaltic flux of a magnetohydrodynamic pseudoplastic nanofluid in a tapered asymmetrical canal. In a nonuniform asymmetric canal, the effects of non-Newtonian fluid and pseudoplastic and dilatancy of this peristaltic flow were examined (Salman & Abdulhadi, 2017; Tahir & Ahmad, 2020). Tripathi & Bég, (2014) researched the effect of nanofluid properties for peristaltic transport. Peristaltic transport of pseudoplastic fluid in a curved channel was investigated by (Hina et al., 2015), who considered all pertinent physical properties as well as the effects of heat and mass transfer. In 2016, Hayat et al., (2016) investigated how thermal radiation and magnetohydrodynamics (MHD) affected the peristaltic transport of a pseudoplastic nanofluid in a tapered asymmetric channel. Without rotation, an inclined porous channel (Salman, 2023) study in 2023 how the impact flow of a pseudoplastic nanofluid in a tapered, asymmetrical inclined porous channel was affected by hydrodynamic and thermal magnetic radiation; however, rotation was not taken into account. Theoretical studies of peristaltic transport in a rotating frame constitute an important area in fluid mechanics, as rotation-induced Coriolis forces can significantly modify momentum transport in geophysical and biomedical systems. Although rotational effects have been studied in various flow configurations, their integration into peristaltic transport models has not been adequately explored, particularly in conjunction with porous media and magnetic fields. Magnetic fields are essential to many therapeutic and medical applications, including magnetotherapy, thermotherapy, arterial blood flow regulation, and cancer treatment. Since rotation's effects and the peristaltic transport mechanism were studied by (Ali & Salman, 2024; Salman et al., 2025), they examined the effects of rotation and magnetic force on the flow of a non-Newtonian fluid through a porous medium. Sh Alshareef, (2020) focused on the Jeffrey fluid's peristaltic transport in a rotating, asymmetrical channel. Abd-Alla & Abo-Dahab, (2016) demonstrated the influence of magnetic force, rotation, and nonlinear heat radiation influences the peristaltic transport of hybrid bio-nanofluids in a symmetric channel (Nassief & Abdulhadi, 2023). Eytan et al., (1999) studied the effect of rotation of non-Newtonian fluids inside a corrugated channel. Although many studies have been conducted on the peristaltic transport of nanofluids and non-Newtonian fluids, the majority of them have focused on specific cases without taking into account the combined effects of rotation, magnetic field, porous medium, and channel inclination. Therefore, in order to provide a deeper understanding of the fluid behavior in such systems, a thorough investigation that takes these factors into account collectively is still required. This study's primary goal is to examine the impacts of magnetohydrodynamics (MHD), porous medium, channel inclination, and rotation on the peristaltic transport of a pseudoplastic nanofluid in an asymmetric rotating inclined channel under boundary conditions. A mathematical model incorporating the momentum, continuity, energy, and concentration equations is developed. The governing equations are transformed into a set of nonlinear ordinary differential equations in dimensionless form using suitable transformations. The analysis is performed under the presumptions of low Reynolds number and long wavelength. Different physical parameters, such as the Hartmann number, thermophoresis parameter, and rotation parameter, are employed to analyze their influence on the velocity distribution, temperature profile, nanoparticle volume function, and pressure rise. Furthermore, the phenomena of trapping and pumping are also examined.

2. Problem Formulation

In this section, the mathematical formulation of the peristaltic transport of pseudoplastic nanofluid under magnetohydrodynamic (MHD) conditions in two dimensions (width $2d$) in an asymmetric rotating inclined channel with a porous medium. Peristaltic waves travel at a speed of c along the $\mathcal{X}$-axis, with the $\mathcal{Y}$-axis perpendicular to it, where $\mathcal{Y}_1$ is the lower wall and $\mathcal{Y}_2$ is the upper wall. In the $\mathcal{Y}$ direction, a homogeneous magnetic field $B = (0, B_0, 0)$ is applied. It is justified to neglect the induced magnetic field since the magnetic Reynolds number is thought to be extremely low. The electric field is also considered absent. The wall surface geometry is specified as follows:

$$\mathcal{Y}_1 = \hat{H}_1 = -d - \mathcal{M}\mathcal{X} - b_1 \sin\left[\frac{2\pi}{\lambda}(\mathcal{X} - c\acute{t}) + \phi\right] \quad (1)$$

$$\mathcal{Y}_2 = \hat{H}_2 = d + \mathcal{M}\mathcal{X} + b_2 \sin\left[\frac{2\pi}{\lambda}(\mathcal{X} - c\acute{t})\right] \quad (2)$$

Where the width of the channel is $2d$ and the parameter ($\mathcal{M} \ll 1$) represents the non-uniformity of the asymmetric tapered channel. The difference phase that varies between $0 \le \phi \le \pi$ is described by ϕ. It has to be observed that when $\phi = 0$, an asymmetric channel with out-of-phase waves come to surface. Moreover, b_1, d, b_2, and ϕ fulfill the following condition:

$$b_1^2 + b_2^2 + 2b_1 b_2 \cos(\phi) \le (2d)^2 \quad (3)$$

In pseudoplastic fluids, the extra stress tensor (Hayat et al., 2012) is:

$$\hat{S} + \lambda_1 \frac{D\hat{S}}{D\acute{t}} + \frac{1}{2}(\lambda_1 - \mu_1)\left(\mathcal{A}_1\hat{S} + \hat{S}\mathcal{A}_1\right) = \mu\mathcal{A}_1$$

Where λ_1 and μ_1 are relaxation times besides $\mathcal{A}_1$ refers to Rivlin-Ericksen tensor. Also:

$$\mathcal{A}_1 = \left[\nabla\vec{V} + \left(\nabla\vec{V}\right)^T\right]$$

The stress components $\hat{S}_{\mathcal{X}\mathcal{X}}, \hat{S}_{\mathcal{X}\mathcal{Y}}$, $\hat{S}_{\mathcal{Y}\mathcal{X}}$ and $\hat{S}_{\mathcal{Y}\mathcal{Y}}$. It can be gained from the following relationships:

$$\begin{aligned}\hat{S}_{\mathcal{X}\mathcal{X}} + \lambda_1\Big[\Big(\frac{\partial}{\partial\acute{t}} + \mathcal{U}\frac{\partial}{\partial\mathcal{X}} + \mathcal{V}\frac{\partial}{\partial\mathcal{Y}}\Big)\hat{S}_{\mathcal{X}\mathcal{X}} \\ - 2\hat{S}_{\mathcal{X}\mathcal{X}}\frac{\partial\mathcal{U}}{\partial\mathcal{X}} 2\hat{S}_{\mathcal{X}\mathcal{Y}}\frac{\partial\mathcal{U}}{\partial\mathcal{Y}}\Big] \\ + \frac{1}{2}(\lambda_1 - \mu_1)\Big[4\hat{S}_{\mathcal{X}\mathcal{X}}\frac{\partial\mathcal{U}}{\partial\mathcal{X}} \\ + 2\hat{S}_{\mathcal{X}\mathcal{Y}}\Big(\frac{\partial\mathcal{U}}{\partial\mathcal{Y}} + \frac{\partial\mathcal{V}}{\partial\mathcal{X}}\Big)\Big] = 2\mu\frac{\partial\mathcal{U}}{\partial\mathcal{X}}\end{aligned} \quad (4)$$

$$\begin{aligned}\hat{S}_{\mathcal{X}\mathcal{Y}} + \lambda_1\Big[\Big(\frac{\partial}{\partial\acute{t}} + \mathcal{U}\frac{\partial}{\partial\mathcal{X}} + \mathcal{V}\frac{\partial}{\partial\mathcal{Y}}\Big)\hat{S}_{\mathcal{X}\mathcal{Y}} - \hat{S}_{\mathcal{X}\mathcal{X}}\frac{\partial\mathcal{V}}{\partial\mathcal{X}} \\ - \hat{S}_{\mathcal{Y}\mathcal{Y}}\frac{\partial\mathcal{U}}{\partial\mathcal{Y}}\Big] \\ + \frac{1}{2}(\lambda_1 - \mu_1)\big(\hat{S}_{\mathcal{X}\mathcal{X}} + \hat{S}_{\mathcal{Y}\mathcal{Y}}\big)\Big(\frac{\partial\mathcal{U}}{\partial\mathcal{Y}} \\ + \frac{\partial\mathcal{V}}{\partial\mathcal{X}}\Big) = \mu\Big(\frac{\partial\mathcal{U}}{\partial\mathcal{Y}} + \frac{\partial\mathcal{V}}{\partial\mathcal{X}}\Big)\end{aligned} \quad (5)$$

$$\begin{aligned}\hat{S}_{\mathcal{Y}\mathcal{Y}} + \lambda_1\Big[\Big(\frac{\partial}{\partial\acute{t}} + \mathcal{U}\frac{\partial}{\partial\mathcal{X}} + \mathcal{V}\frac{\partial}{\partial\mathcal{Y}}\Big)\hat{S}_{\mathcal{Y}\mathcal{Y}} - 2\hat{S}_{\mathcal{X}\mathcal{Y}}\frac{\partial\mathcal{V}}{\partial\mathcal{X}} \\ - 2\hat{S}_{\mathcal{Y}\mathcal{Y}}\frac{\partial\mathcal{V}}{\partial\mathcal{Y}}\Big] \\ + \frac{1}{2}(\lambda_1 - \mu_1)\Big[2\hat{S}_{\mathcal{X}\mathcal{Y}}\Big(\frac{\partial\mathcal{U}}{\partial\mathcal{Y}} + \frac{\partial\mathcal{V}}{\partial\mathcal{X}}\Big) \\ + 4\hat{S}_{\mathcal{Y}\mathcal{Y}}\frac{\partial\mathcal{V}}{\partial\mathcal{Y}}\Big] = 2\mu\frac{\partial\mathcal{V}}{\partial\mathcal{Y}}\end{aligned} \quad (6)$$

3. Method of Solution

The continuity equation:

$$\frac{\partial\mathcal{U}}{\partial\mathcal{X}} + \frac{\partial\mathcal{V}}{\partial\mathcal{Y}} = 0$$

The momentum equations:

$$\begin{aligned}\rho_f\Big[\frac{\partial\mathcal{U}}{\partial\acute{t}} + \mathcal{U}\frac{\partial\mathcal{U}}{\partial\mathcal{X}} + \mathcal{V}\frac{\partial\mathcal{U}}{\partial\mathcal{Y}}\Big] = -\frac{\partial\tilde{P}}{\partial\mathcal{X}} + \frac{\partial}{\partial\mathcal{X}}(\hat{S}_{\mathcal{X}\mathcal{X}}) \\ + \frac{\partial}{\partial\mathcal{Y}}(\hat{S}_{\mathcal{X}\mathcal{Y}}) - \acute{\sigma}B_0^2\mathcal{U} - \frac{\mu}{K_0}\mathcal{U} \\ + \rho_f g\sin\alpha + \Omega\rho_f(\Omega\mathcal{U} + 2\mathcal{V})\end{aligned} \quad (8)$$

$$\begin{aligned}\rho_f\Big[\frac{\partial\mathcal{V}}{\partial\acute{t}} + \mathcal{U}\frac{\partial\mathcal{V}}{\partial\mathcal{X}} + \mathcal{V}\frac{\partial\mathcal{V}}{\partial\mathcal{Y}}\Big] = -\frac{\partial\tilde{P}}{\partial\mathcal{Y}} + \frac{\partial}{\partial\mathcal{X}}(\hat{S}_{\mathcal{Y}\mathcal{X}}) \\ + \frac{\partial}{\partial\mathcal{Y}}(\hat{S}_{\mathcal{Y}\mathcal{Y}}) - \frac{\mu}{K_0}\mathcal{V} - \rho_f g\cos\alpha + \Omega\rho_f(\Omega\mathcal{V} - 2\mathcal{U})\end{aligned} \quad (9)$$

The nanoparticle temperature governing equation is:

$$\begin{aligned}(\rho\acute{c})_f\Big[\frac{\partial\mathcal{T}}{\partial\acute{t}} + \mathcal{U}\frac{\partial\mathcal{T}}{\partial\mathcal{X}} + \mathcal{V}\frac{\partial\mathcal{T}}{\partial\mathcal{Y}}\Big] \\ = \kappa\Big[\frac{\partial^2\mathcal{T}}{\partial\mathcal{X}^2} + \frac{\partial^2\mathcal{T}}{\partial\mathcal{Y}^2}\Big] \\ + (\rho\acute{c})_p\frac{D_T}{T_m}\Big[\Big(\frac{\partial\mathcal{T}}{\partial\mathcal{X}}\Big)^2 + \Big(\frac{\partial\mathcal{T}}{\partial\mathcal{Y}}\Big)^2\Big] \\ + (\rho\acute{c})_p D_B\Big(\frac{\partial\mathcal{C}}{\partial\mathcal{X}}\frac{\partial\mathcal{T}}{\partial\mathcal{X}} \\ + \frac{\partial\mathcal{C}}{\partial\mathcal{Y}}\frac{\partial\mathcal{T}}{\partial\mathcal{Y}}\Big) + Q_0 - \frac{\partial q_r}{\partial\mathcal{Y}}\end{aligned} \quad (10)$$

The concentration governing equation is:

$$\left[\frac{\partial \mathcal{C}}{\partial \acute{t}}+\mathcal{U}\frac{\partial \mathcal{C}}{\partial \mathcal{X}}+\mathcal{V}\frac{\partial \mathcal{C}}{\partial \mathcal{Y}}\right] = D_B\left(\frac{\partial^2 \mathcal{C}}{\partial \mathcal{X}^2}+\frac{\partial^2 \mathcal{C}}{\partial \mathcal{Y}^2}\right) + \frac{D_T}{T_m}\left(\frac{\partial^2 \mathcal{T}}{\partial \mathcal{X}^2}+\frac{\partial^2 \mathcal{T}}{\partial \mathcal{Y}^2}\right) \quad (11)$$

Symbols $\mathcal{V}$ and $\mathcal{U}$ denote the transverse and axial velocity components, respectively.

The Radiative heat flux:

$$q_r = -\frac{16\,\sigma^*\,{T_0}^3}{3\mathcal{K}^*}\cdot\frac{\partial \mathcal{T}}{\partial \mathcal{Y}}$$

A special table called NOMENCLATURE defines some of the symbols used in this analysis.

The no-slip and convective thermal boundaries are among the governing boundary constraints, which can be expressed as follows:

$$U=0\,,\quad \mathcal{T}=T_0 \quad and\, \mathcal{C}=C_0 \;\; at \;\; \mathcal{Y}_1=\check{H}_1 \quad (12)$$

$$U=0\,,\quad \mathcal{T}=T_1 \;\; and \;\; \mathcal{C}=C_1 \quad at \;\; \mathcal{Y}_2=\check{H}_2 \quad (13)$$

To simplify the formulation, the nondimensional variable is defined as follows:

$$\left.\begin{aligned} x=\frac{\varkappa}{\lambda}\,,\quad \mathcal{y}=\frac{\mathcal{Y}}{d}\,,t=\frac{c\acute{t}}{\lambda}\,,u=\frac{\mathcal{u}}{c}\,,\\ v=\frac{\mathcal{v}}{c}\,,\delta=\frac{d}{\lambda}\,,\quad \sigma=\frac{\mathcal{C}-C_0}{C_1-C_0}\\ \hbar_2=\frac{\check{H}_2}{d},\theta=\frac{\mathcal{T}-T_0}{T_1-T_0}\,,p=\frac{d^2\tilde{p}}{\lambda\mu c},\\ S_{ij}=\frac{d_1}{c\mu}\hat{S}_{i\,j},\quad \lambda_1^*=\frac{\lambda_1 c}{d}\,,Pr=\frac{\mu\acute{c}_f}{k}\\ K=\frac{K_0}{d^2},\quad Re=\frac{\rho_f c d}{\mu},\quad a=\frac{b_1}{d},\\ b=\frac{b_2}{d}\,,\quad m=\frac{\mathcal{M}\lambda}{d}\,,Sr=\frac{K_T D_B(T_1-T_0)}{T_m\;v\,(C_1-C_0)}\\ Nt=\frac{\tau D_T(T_1-T_0)}{T_m\,\mathcal{v}},M=\sqrt{\frac{\acute{\sigma}}{\mu}}dB_0,\quad Fr=\frac{c^2}{gd},\\ u=\frac{\partial \psi}{\partial y}\,,Sc=\frac{v}{D_B}\,,Ta=\frac{\Omega Red}{c}\\ \hbar_1=\frac{\check{H}_1}{d},\mu_1^*=\frac{\mu_1 c}{d},v=-\delta\frac{\partial \psi}{\partial x},\\ \beta=\frac{d^2\;Q_0}{(T_1-T_0)\mu\acute{c}_f}\,,R_n=\frac{16\;\sigma^*\,{T_0}^3}{3\mathcal{K}^*\,\mu\acute{c}_f} \end{aligned}\right\} \quad (14)$$

Where the dimensionless parameters refer to the following quantities: $\mathcal{y}$ and x denote the axial and transverse coordinates, for the Froude number,ψ the stream function, $\hbar_2$ the positions of upper wall and $\hbar_1$ the positions of lower wall, v and u are the velocity components in the transverse and axial directions.

A moving coordinate system (X,Y) will be described, propagating along the X-axis with the same velocity c wave. In both frames, the velocity and pressure components and coordinates are as follows:

$$\left.\begin{aligned} \varkappa=\mathcal{X}\;-c\acute{t}\,,\mathcal{Y}=\mathcal{X},u(\varkappa,\mathcal{Y})=\mathcal{U}(\mathcal{X}\,,\mathcal{Y},\acute{t})-c,\\ v(\varkappa,\mathcal{Y})=\mathcal{V}(\mathcal{X}\,,\mathcal{Y},\acute{t}),\tilde{p}(\varkappa,\mathcal{Y})=\tilde{P}(\mathcal{X}\,,\mathcal{Y},\acute{t}) \end{aligned}\right\} \quad (15)$$

The continuity is satisfying and the Equations (8-11) become:

$$\begin{aligned} Re\delta\left[\left(\frac{\partial \psi}{\partial \mathcal{y}}+1\right)\frac{\partial^2\psi}{\partial x\partial \mathcal{y}}-\frac{\partial \psi}{\partial x}\frac{\partial^2\psi}{\partial \mathcal{y}^2}\right] &= -\frac{\partial p}{\partial x}+\delta\frac{\partial}{\partial x}(S_{xx})\\ &+\frac{\partial}{\partial \mathcal{y}}(S_{x\mathcal{y}})-\left(M^2+\frac{1}{K}\right)\left(\frac{\partial \psi}{\partial \mathcal{y}}+1\right)\\ &+\frac{Re}{Fr}sin\alpha+k_r\left(\frac{\partial \psi}{\partial \mathcal{y}}+1\right)-2\delta\,Ta\,\frac{\partial \psi}{\partial x} \end{aligned} \quad (16)$$

$$\begin{aligned} -Re\delta^3\left[\left(\frac{\partial \psi}{\partial \mathcal{y}}+1\right)\frac{\partial^2\psi}{\partial x^2}+\frac{\partial \psi}{\partial x}\frac{\partial^2\psi}{\partial x\partial \mathcal{y}}\right] &= -\frac{\partial p}{\partial \mathcal{y}}+\delta^2\frac{\partial}{\partial x}(S_{x\mathcal{y}})\\ +\delta\frac{\partial}{\partial \mathcal{y}}(S_{\mathcal{y}\mathcal{y}})+\frac{\delta^2}{K}\frac{\partial \psi}{\partial x}-\delta\frac{Re}{Fr}cos\alpha-k_r\delta^2\frac{\partial \psi}{\partial x}&\\ -2\delta Ta\left(\frac{\partial \psi}{\partial \mathcal{y}}+1\right)& \end{aligned} \quad (17)$$

Where $k_r=\frac{\Omega^2 d}{c}Re.$

$$\begin{aligned} Re\delta\left[\left(\frac{\partial \psi}{\partial \mathcal{y}}+1\right)\frac{\partial \theta}{\partial x}-\frac{\partial \psi}{\partial x}\frac{\partial \theta}{\partial \mathcal{y}}\right] &= \frac{1}{Pr}\left[\delta^2\frac{\partial^2\theta}{\partial x^2}+\frac{\partial^2\theta}{\partial \mathcal{y}^2}\right]\\ &+N_b\left(\delta^2\frac{\partial \sigma}{\partial x}\frac{\partial \theta}{\partial x}+\frac{\partial \sigma}{\partial \mathcal{y}}\frac{\partial \theta}{\partial \mathcal{y}}\right)\\ &+Nt\left[\delta^2\left(\frac{\partial \theta}{\partial x}\right)^2+\left(\frac{\partial \theta}{\partial \mathcal{y}}\right)^2\right]+\beta\\ &+R_n\frac{\partial^2\theta}{\partial \mathcal{y}^2} \end{aligned} \quad (18)$$

$$\begin{aligned} Re\delta\left[\left(\frac{\partial \psi}{\partial \mathcal{y}}+1\right)\frac{\partial \sigma}{\partial x}-\frac{\partial \psi}{\partial x}\frac{\partial \sigma}{\partial \mathcal{y}}\right] &= \frac{1}{Sc}\left[\delta^2\frac{\partial^2\sigma}{\partial x^2}+\frac{\partial^2\sigma}{\partial \mathcal{y}^2}\right]\\ &+\frac{Nt}{Sc\;N_b}\left(\delta^2\frac{\partial^2\theta}{\partial x^2}+\frac{\partial^2\theta}{\partial \mathcal{y}^2}\right) \end{aligned} \quad (19)$$

The dimensionless stress components (4-6) are:

$$S_{xx} + \lambda_1^* \left\{ \delta \left[\frac{\partial}{\partial t} + \left(\frac{\partial \psi}{\partial y} + 1 \right) \frac{\partial}{\partial x} - \frac{\partial \psi}{\partial x} \frac{\partial}{\partial y} \right] S_{xx} - 2\delta S_{xx} \frac{\partial^2 \psi}{\partial x \partial y} - 2 S_{xy} \frac{\partial^2 \psi}{\partial y^2} \right\} + \frac{1}{2} (\lambda_1^* - \mu_1^*) \left[4\delta S_{xx} \frac{\partial^2 \psi}{\partial x \partial y} + 2 S_{xy} \left(\frac{\partial^2 \psi}{\partial y^2} - \delta^2 \frac{\partial^2 \psi}{\partial x^2} \right) \right] = 2\delta \frac{\partial^2 \psi}{\partial x \partial y} \tag{20}$$

$$S_{xy} + \lambda_1^* \left\{ \delta \left[\frac{\partial}{\partial t} + \left(\frac{\partial \psi}{\partial y} + 1 \right) \frac{\partial}{\partial x} - \frac{\partial \psi}{\partial x} \frac{\partial}{\partial y} \right] S_{xy} + \delta^2 S_{xx} \frac{\partial^2 \psi}{\partial x^2} - S_{yy} \frac{\partial^2 \psi}{\partial y^2} \right\} + \frac{1}{2} (\lambda_1^* - \mu_1^*) (S_{xx} + S_{yy}) \left(\frac{\partial^2 \psi}{\partial y^2} - \delta^2 \frac{\partial^2 \psi}{\partial x^2} \right) = \frac{\partial^2 \psi}{\partial y^2} - \delta^2 \frac{\partial^2 \psi}{\partial x^2} \tag{21}$$

$$S_{yy} + \lambda_1^* \left\{ \delta \left[\frac{\partial}{\partial t} + \left(\frac{\partial \psi}{\partial y} + 1 \right) \frac{\partial}{\partial x} - \frac{\partial \psi}{\partial x} \frac{\partial}{\partial y} \right] S_{yy} - 2\delta^2 S_{xy} \frac{\partial^2 \psi}{\partial x^2} + 2\delta S_{yy} \frac{\partial^2 \psi}{\partial x \partial y} \right\} + \frac{1}{2} (\lambda_1^* - \mu_1^*) \left[-4\delta S_{yy} \frac{\partial^2 \psi}{\partial x \partial y} + 2 S_{xy} \left(\frac{\partial^2 \psi}{\partial y^2} - \delta^2 \frac{\partial^2 \psi}{\partial x \partial y} \right) \right] = -2\delta \frac{\partial^2 \psi}{\partial x \partial y} \tag{22}$$

Similarly, Equations (12) and (13) can be written like this:

$$\frac{\partial \psi}{\partial y} = 0, \quad \theta = 0 \ \ and \ \sigma = 0 \quad at \quad y = \hbar_1 \tag{23}$$

$$\frac{\partial \psi}{\partial y} = 0, \quad \theta = 1 \ \ and \ \sigma = 1 \quad at \quad y = \hbar_2 \tag{24}$$

Using the long wavelength approximation and the small Reynolds number limit are used, Equations (16-22) become:

$$\frac{\partial p}{\partial x} = \frac{\partial}{\partial y} (S_{xy}) - \left(M^2 + \frac{1}{K} \right) \left(\frac{\partial \psi}{\partial y} + 1 \right) + \frac{Re}{Fr} sin\alpha + k_r \left(\frac{\partial \psi}{\partial y} + 1 \right) \tag{25}$$

$$\frac{\partial p}{\partial y} = 0 \tag{26}$$

$$\frac{\partial^2 \theta}{\partial y^2} + N_b Pr \left(\frac{\partial \sigma}{\partial y} \frac{\partial \theta}{\partial y} \right) + Pr \, Nt \left(\frac{\partial \theta}{\partial y} \right)^2 + Pr\beta + PrR_n \frac{\partial^2 \theta}{\partial y^2} = 0 \tag{27}$$

$$\frac{\partial^2 \sigma}{\partial y^2} + \frac{Nt}{N_b} \frac{\partial^2 \theta}{\partial y^2} = 0 \tag{28}$$

$$S_{xx} = (\lambda_1^* + \mu_1^*) S_{xy} \frac{\partial^2 \psi}{\partial y^2} \tag{29}$$

$$S_{xy} + \frac{1}{2} (\lambda_1^* - \mu_1^*) (S_{xx} + S_{yy}) \frac{\partial^2 \psi}{\partial y^2} - \lambda_1^* S_{yy} \frac{\partial^2 \psi}{\partial y^2} = \frac{\partial^2 \psi}{\partial y^2} \tag{30}$$

$$S_{yy} = -(\lambda_1^* - \mu_1^*) S_{xy} \frac{\partial^2 \psi}{\partial y^2} \tag{31}$$

Since Equation (26) shows that P is independent of y, pressure can be removed from Equation (25), and adding the pseudoplastic fluid parameter $\Sigma = (\lambda_1^* - \mu_1^*)$, the following system is obtained:

$$\frac{\partial^2}{\partial y^2} (S_{xy}) - \left(M^2 + \frac{1}{K} \right) \frac{\partial^2 \psi}{\partial y^2} + k_r \left(\frac{\partial^2 \psi}{\partial y^2} \right) = 0 \tag{32}$$

$$S_{xy} = \frac{\partial^2 \psi}{\partial y^2} \left(1 - \Sigma \left(\frac{\partial^2 \psi}{\partial y^2} \right)^2 \right)^{-1} \tag{33}$$

Subject to the boundary constraints:

$$\psi = -\frac{F}{2}, \frac{\partial \psi}{\partial y} = 0 \, , \theta = 0 \ and \ \sigma = 0 \ \ at \ y = \hbar_1 = -1 - m(x + t) - b \, sin[2\pi x + \phi] \tag{34}$$

$$\psi = \frac{F}{2}, \frac{\partial \psi}{\partial y} = 0, \theta = 1 \ and \ \sigma = 1 \ at \ y = \hbar_2 = 1 + m(x + t) + a \, sin[2\pi x] \tag{35}$$

The dimensionless form of mean flows is represented by the symbol F.

$$F(x, t) = Q + b \, sin[2\pi x] + a \, sin[2\pi x + \phi] \tag{36}$$

$$F = \int_{\hbar_1(x)}^{\hbar_2(x)} \frac{\partial \psi}{\partial y}, Q \equiv \frac{\tilde{q}}{cd}, dy = \psi(\hbar_2) - \psi(\hbar_1) \tag{37}$$

The following formula yields the pressure rise per wavelength:

$$\Delta p = \int_0^1 \frac{\partial p}{\partial \boldsymbol{x}} d\boldsymbol{x} \tag{38}$$

The boundary constraints (Equations (34 and 35)) and Equations (27, 28, 32 and 33). Analytical expressions for the temperature field, heat transfer rate,

stream function, axial velocity, pressure distribution, pressure gradient, and nanoparticle concentration were obtained using the perturbation method in the numerical solution.

4. Solution Technique

Numerical approaches are used because Equations (27, 28, 32 and 33) cannot be solved exactly using traditional methods. The perturbation technique is being used to compute analytical series solutions corresponding to small governing parameters. In particular, the pseudoplastic fluid parameter is assumed to be sufficiently small, which is a physically plausible assumption for many real-world pseudoplastic fluids, particularly in biofluid applications. Analytical solutions for complex flow models have been obtained using the perturbation method, which has been shown to be both robust and effective in similar studies (Hina et al., 2015; Salman & Abdulhadi, 2018). Using the perturbation method in this context to derive the series solutions corresponding to small parameters. The perturbation expansion is carried out with respect to the small fluid parameter Σ for the variables P, ψ, F while the Prandtl number Pr for the variables θ and σ. The series expansions are kept up to the first-order approximation after being truncated.

$$\left.\begin{array}{c} P = P_0 + \Sigma P_1 + \Sigma^2 P_2 + \cdots , \\ \psi = \psi_0 + \Sigma \psi_1 + \Sigma^2 \psi_2 + \cdots , \\ F = F_0 + \Sigma F_1 + \Sigma^2 F_2 + \cdots , \\ \sigma = \sigma_0 + Pr\sigma_1 + Pr^2\sigma_2 + \cdots , \\ \theta = \theta_0 + Pr\theta_1 + Pr^2\theta_2 + \cdots \end{array}\right\} \quad (39)$$

4. 1. Zeroth-Order Equations

$$\frac{\partial^4 \psi_0}{\partial y^4} - {N_1}^2 \frac{\partial^2 \psi_0}{\partial y^2} + k_r \frac{\partial^2 \psi_0}{\partial y^2} = 0 \quad (40)$$

$$\frac{\partial^2 \theta_0}{\partial y^2} = 0 \quad (41)$$

$$\frac{\partial^2 \sigma_0}{\partial y^2} + \frac{Nt}{N_b}\frac{\partial^2 \theta_0}{\partial y^2} = 0 \quad (42)$$

$$\frac{\partial p_0}{\partial x} = \frac{\partial^3 \psi_0}{\partial y^3} - {N_1}^2\left(\frac{\partial \psi_0}{\partial y} + 1\right) + \frac{Re}{Fr} sin\alpha + k_r\left(\frac{\partial \psi_0}{\partial y} + 1\right) \quad (43)$$

Whereas (${N_1}^2 = M^2 + \frac{1}{K}$ and $A = k_r$) consider the following boundary constraints:

$$\psi_0 = -\frac{F_0}{2}, \frac{\partial \psi_0}{\partial y} = 0, \theta_0 = 0 \ and \ \sigma_0 = 0 \ at \ y = \hbar_1 \quad (44)$$

$$\psi_0 = \frac{F_0}{2}, \frac{\partial \psi_0}{\partial y} = 0, \ \theta_0 = 1 \ and \ \sigma_0 = 1 \ at \ y = \hbar_2 \quad (45)$$

Solutions equation are:

$$\psi_0 = c_3 + y c_4 + \frac{e^{-y\sqrt{A+N_1^2}}(c_1 + e^{2y\sqrt{A+N_1^2}}c_2)}{A + N_1^2}$$

$$\theta_0 = \frac{\hbar_1}{\hbar_1 - \hbar_2} - \frac{y}{\hbar_1 - \hbar_2}$$

$$\sigma_0 = \frac{\hbar_1 - y}{\hbar_1 - \hbar_2}$$

$$\frac{\partial p_0}{\partial x} = \frac{Re\ Sin[\alpha]}{Fr} + 2c_2 e^{y\sqrt{A+N_1^2}}\sqrt{A+N_1^2} - e^{-y\sqrt{A+N_1^2}}(c_1 + c_2 e^{2y\sqrt{A+N_1^2}})\sqrt{A+N_1^2} - A(1 + c_4 + \frac{2c_2 e^{y\sqrt{A+N_1^2}}}{\sqrt{A+N_1^2}} - \frac{e^{-y\sqrt{A+N_1^2}}(c_1 + c_2 e^{2y\sqrt{A+N_1^2}})}{\sqrt{A+N_1^2}}) - N_1^2(1 + c_4 + \frac{2c_2 e^{y\sqrt{A+N_1^2}}}{\sqrt{A+N_1^2}} - \frac{e^{-y\sqrt{A+N_1^2}}(c_1 + c_2 e^{2y\sqrt{A+N_1^2}})}{\sqrt{A+N_1^2}})$$

4. 2. First-Order Equations

$$\frac{\partial^4 \psi_1}{\partial y^4} + 3\frac{\partial^4 \psi_0}{\partial y^4}\left(\frac{\partial^2 \psi_0}{\partial y^2}\right)^2 + 6\left(\frac{\partial^3 \psi_0}{\partial y^3}\right)^2\left(\frac{\partial^2 \psi_0}{\partial y^2}\right) - {N_1}^2\frac{\partial^2 \psi_1}{\partial y^2} + k_r \frac{\partial^2 \psi_1}{\partial y^2} = 0 \quad (46)$$

$$\frac{\partial^2 \theta_1}{\partial y^2} + N_b\frac{\partial \sigma_0}{\partial y}\frac{\partial \theta_0}{\partial y} + Nt\left(\frac{\partial \theta_0}{\partial y}\right)^2 + \beta + R_n\frac{\partial^2 \theta_0}{\partial y^2} = 0 \quad (47)$$

$$\frac{\partial^2 \sigma_1}{\partial y^2} + \frac{Nt}{N_b}\frac{\partial^2 \theta_1}{\partial y^2} = 0 \quad (48)$$

$$\frac{\partial p_1}{\partial x} - \frac{\partial^3 \psi_1}{\partial y^3} - 3\frac{\partial^3 \psi_0}{\partial y^3}\left(\frac{\partial^2 \psi_0}{\partial y^2}\right)^2 + {N_1}^2\frac{\partial \psi_1}{\partial y} + k_r\frac{\partial \psi_1}{\partial y} = 0 \quad (49)$$

Considering the following boundary constraints:

$$\psi_1 = -\frac{F_1}{2}, \frac{\partial \psi_1}{\partial y} = 0, \theta_1 = 0 \ and \ \sigma_1 = 0 \ at \ y = \hbar_1 \quad (50)$$

$$\psi_1 = \frac{F_1}{2}, \frac{\partial \psi_1}{\partial y} = 0, \theta_1 = 0 \; and \; \sigma_1 = 0 \; at \; y = \hbar_2 \qquad (51)$$

Solutions equation are:

$$\psi_1 = c_7 + y c_8 + \frac{1}{8(A+N_1^2)} e^{-3y\sqrt{A+N_1^2}} (-{c_1}^3 + 30{c_1}^2 c_2 e^{2y\sqrt{A+N_1^2}} + 30 c_1 {c_2}^2 e^{4y\sqrt{A+N_1^2}} - {c_2}^3 e^{6y\sqrt{A+N_1^2}} + 8e^{2y\sqrt{A+N_1^2}} c_5 + 8e^{4y\sqrt{A+N_1^2}} c_6 - 6c_1 c_2 e^{2y\sqrt{A+N_1^2}} (-c_1 + c_2 e^{2y\sqrt{A+N_1^2}}) Log[e^{2y\sqrt{A+N_1^2}}])$$

$$\theta_1 = -\frac{{\hbar_1}^2 y^2 \beta}{2(\hbar_1-\hbar_2)^2} + \frac{\hbar_1 \hbar_2 y^2 \beta}{(\hbar_1-\hbar_2)^2} - \frac{{\hbar_2}^2 y^2 \beta}{2(\hbar_1-\hbar_2)^2} - \frac{{\hbar_1}^3 \hbar_2 \beta - 2{\hbar_1}^2 {\hbar_2}^2 \beta + \hbar_1 {\hbar_2}^3 \beta + {\hbar_1}^3 \hbar_2 N_b + {\hbar_1}^3 \hbar_2 N_t}{2(\hbar_1-\hbar_2)^2} + y\left(-\frac{-{\hbar_1}^3 \beta + {\hbar_1}^2 \hbar_2 \beta + \hbar_1 {\hbar_2}^2 \beta - {\hbar_2}^3 \beta - {\hbar_1}^3 N_b}{2(\hbar_1-\hbar_2)^2} - \frac{-{\hbar_1}^2 \hbar_2 N_b - {\hbar_1}^3 N_t - {\hbar_1}^2 \hbar_2 N_t}{2(\hbar_1-\hbar_2)^2}\right) - \frac{{\hbar_1}^2 y^2 N_b}{2(\hbar_1-\hbar_2)^2} - \frac{{\hbar_1}^2 y^2 N_t}{2(\hbar_1-\hbar_2)^2}$$

$$\sigma_1 = -\frac{-{\hbar_1}^3 \hbar_2 \beta N_t + 2{\hbar_1}^2 {\hbar_2}^2 \beta N_t - \hbar_1 {\hbar_2}^3 \beta N_t - {\hbar_1}^3 \hbar_2 N_b N_t - {\hbar_1}^3 \hbar_2 N_t^2}{2(\hbar_1-\hbar_2)^2 N_b} + y\left(-\frac{{\hbar_1}^3 \beta N_t - {\hbar_1}^2 \hbar_2 \beta N_t - \hbar_1 {\hbar_2}^2 \beta N_t + {\hbar_2}^3 \beta N_t + {\hbar_1}^3 N_b N_t + {\hbar_1}^2 \hbar_2 N_b N_t + {\hbar_1}^3 N_t^2 + {\hbar_1}^2 \hbar_2 N_t^2}{2(\hbar_1-\hbar_2)^2 N_b}\right) + \frac{{\hbar_1}^2 y^2 N_t}{2(\hbar_1-\hbar_2)^2} + \frac{{\hbar_1}^2 y^2 \beta N_t}{2(\hbar_1-\hbar_2)^2 N_b} - \frac{\hbar_1 \hbar_2 y^2 \beta N_t}{(\hbar_1-\hbar_2)^2 N_b} + \frac{{\hbar_2}^2 y^2 \beta N_t}{2(\hbar_1-\hbar_2)^2 N_b} + \frac{{\hbar_1}^2 y^2 N_t^2}{2(\hbar_1-\hbar_2)^2 N_b}$$

$$\frac{\partial p_1}{\partial x} = -\frac{27}{8} e^{-3y\sqrt{A+N_1^2}} \left(-{c_1}^3 + 30{c_1}^2 c_2 e^{2y\sqrt{A+N_1^2}} + 8c_5 e^{2y\sqrt{A+N_1^2}} + 30 c_1 {c_2}^2 e^{4y\sqrt{A+N_1^2}} + 8c_6 e^{4y\sqrt{A+N_1^2}} - {c_2}^3 e^{6y\sqrt{A+N_1^2}} - 6c_1 c_2 e^{2y\sqrt{A+N_1^2}} \left(-c_1 + c_2 e^{2y\sqrt{A+N_1^2}}\right) Log\left[e^{2y\sqrt{A+N_1^2}}\right]\right) \sqrt{A+N_1^2} + \cdots$$

5. Results And Discussion

This part of the study reviews the influences of different physical parameters on flow properties using graphs and numerical results. Trapping, velocity distribution, and pressure rise are all examined in the analysis. It is shown that these behaviors are affected by increasing the values of parameters such as Hartmann number (M), phase difference coefficient (ϕ), flow rate (Q), non-uniform parameter (m), the Prandtl number Pr, the thermophoresis parameter Nt and rotation parameter (Ω)

5. 1. Trapping

Figures 1-8 show the trapping phenomenon corresponding to different values of (m), (M), (ϕ), and (Q). It has been noticed that the size of the trapped bolus increases with (Q) and (M). This growth is attributed to the enlargement of the expansion zones, which promotes the formation of larger closed streamlines. It is also seen that the volume of the trapped mass decreases as (ϕ) and (m) increases.

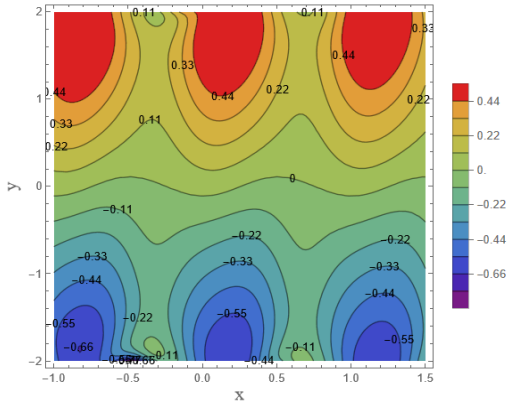

Figure 1. Stream lines for $a = 0.31, b = 0.21, \Sigma = 0.11, k = 0.31, \Omega = 0.2, d = 1, \rho = 0.1, \mu = 0.1, Q = 0.84, \phi = \frac{\pi}{4}, t = 6.01, m = 0.11, M = 3.41.$

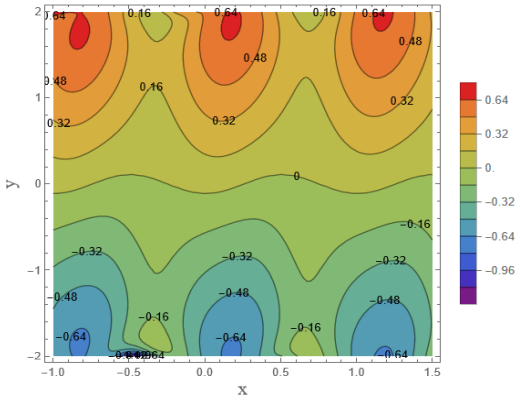

Figure 2. Stream lines for $a = 0.31, b = 0.21, \Sigma = 0.11, k = 0.31, \Omega = 0.2, d = 1, \rho = 0.1, \mu = 0.1, Q = 0.84, \phi = \frac{\pi}{4}, t = 6.01, m = 0.11, M = 3.61.$

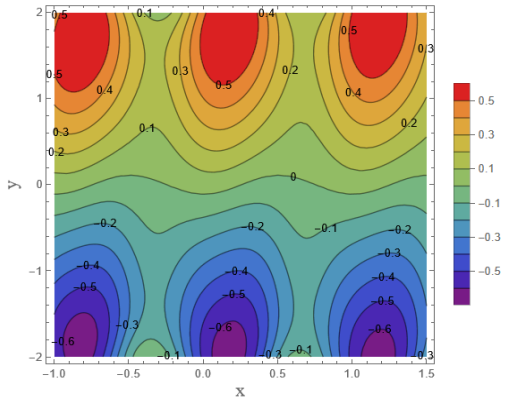

Figure 3. Stream lines for $a = 0.31, b = 0.21, \Sigma = 0.11, k = 0.31, \Omega = 1, d = 1, \rho = 1, \mu = 1, Q = 0.84, t = 6.01, m = 0.11, M = 2.21, \phi = \frac{\pi}{4}$.

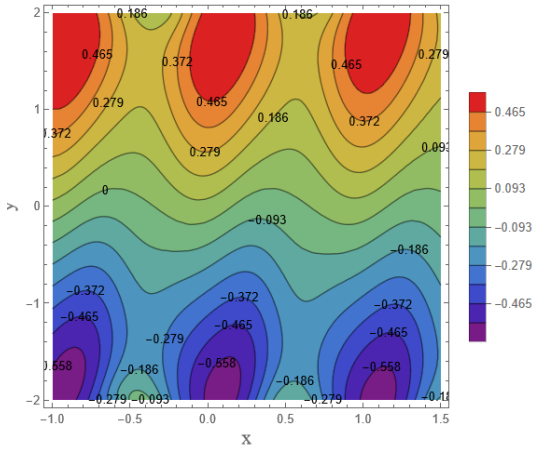

Figure 4. Stream lines for $a = 0.31, b = 0.21, \Sigma = 0.11, k = 0.31, \Omega = 1, d = 1, \rho = 1, \mu = 1, Q = 0.84, t = 6.01, m = 0.11, M = 2.21, \phi = \frac{\pi}{2}$.

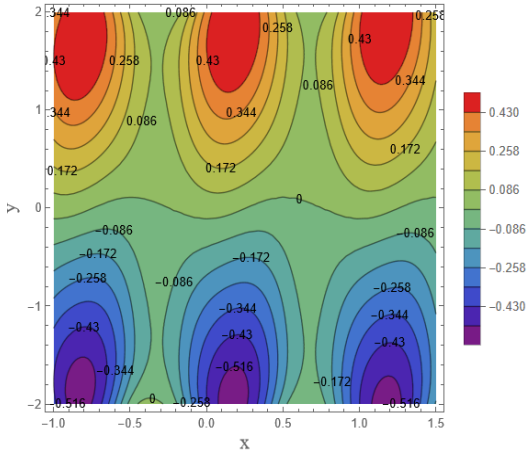

Figure 5. Stream lines for $a = 0.31, b = 0.21, \Sigma = 0.11, k = 0.31, \Omega = 1, d = 1, \rho = 1, \mu = 1, t = 6.01, m = 0.11, M = 2.21, \phi = \frac{\pi}{4}, Q = 0.64$.

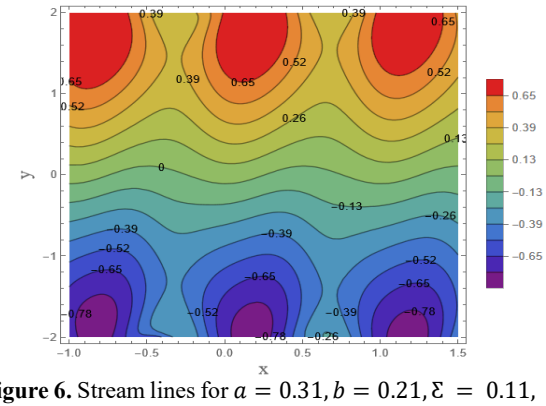

Figure 6. Stream lines for $a = 0.31, b = 0.21, \Sigma = 0.11, k = 0.31, \Omega = 1, d = 1, \rho = 1, \mu = 1, t = 6.01, m = 0.11, M = 2.21, \phi = \frac{\pi}{4}, Q = 1.24$.

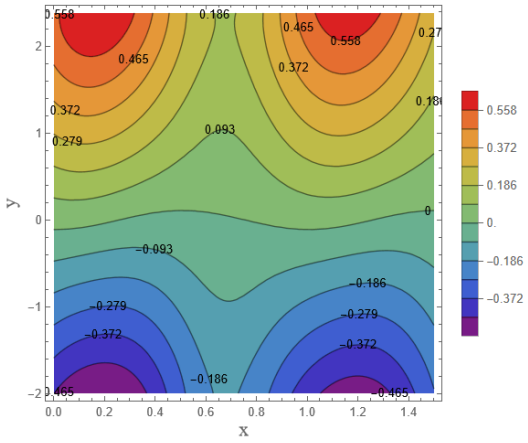

Figure 7. Stream lines for $a = 0.31, b = 0.21, \Sigma = 0.11, k = 0.31, \Omega = 0.1, d = 1, \rho = 0.1, \mu = 0.1, t = 6.01, M = 2.21, \phi = \frac{\pi}{4}, Q = 0.84, m = 0.22$.

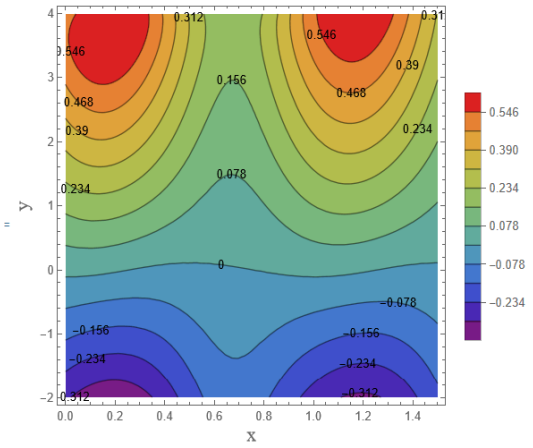

Figure 8. Stream lines for $a = 0.31, b = 0.21, \Sigma = 0.11, k = 0.31, \Omega = 0.1, d = 1, \rho = 0.1, \mu = 0.1, t = 6.01, M = 2.21, \phi = \frac{\pi}{4}, Q = 0.84, m = 0.43$.

5. 2. Velocity Profile

First, it is evident from the graphs in Figures 9-12 that the velocity distribution takes the shape of a parabola. Plotting these figures allowed the examination of how the velocity profile was affected by the (M), (ϕ), (Q) and (Ω). Figure 9 illustrates how velocity is affected by the (M). The findings indicate that velocity increases in the center channel while an inverse trend is seen close to the boundaries. This is explained by the applied magnetic field's influence, which hinders fluid motion and acts as an axial damping force to lower flow velocity. As the rotation parameter (Ω) increases, Figure 12 illustrates the velocity increases in the center channel while decreases to the boundaries. The velocity increases gradually as (ϕ) rises, as shown in Figure 10. As seen in Figure 11, the velocity gradually decreases as the flow rate (Q) increases.

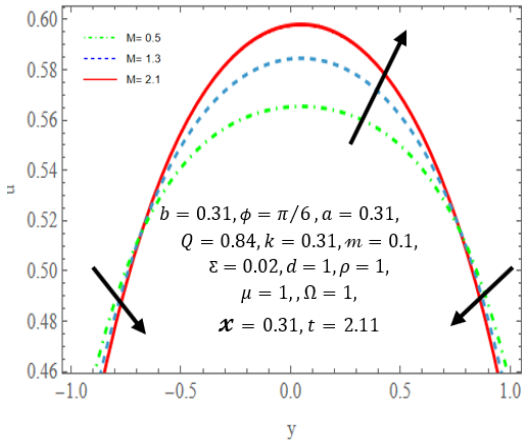

Figure 9. Different values to (M) on the velocity profile.

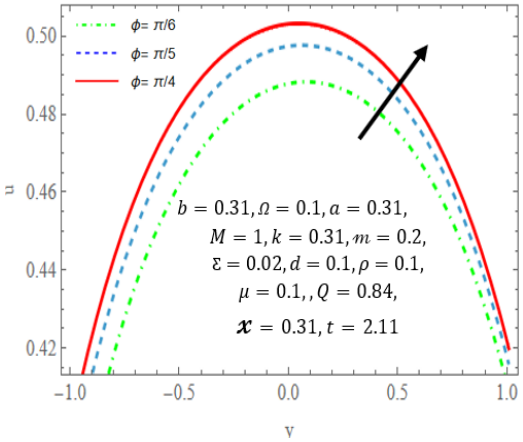

Figure 10. Different values to (ϕ) on the velocity profile.

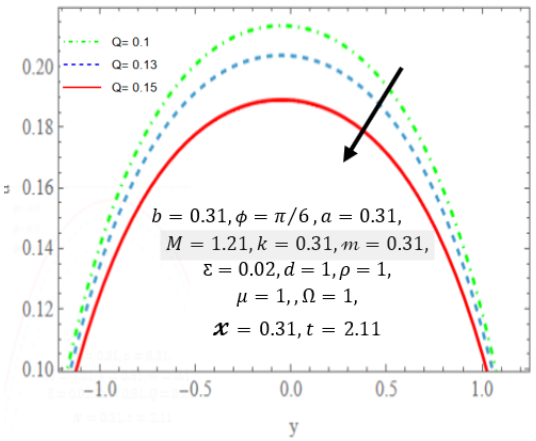

Figure 11. Different values to(Q) on the velocity profile.

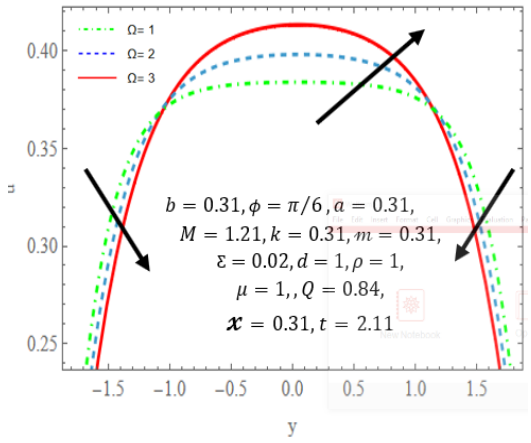

Figure 12. Different values to (Ω) on the velocity profile.

5. 3. Pumping Characteristics

The average pressure rise is influenced by various physical parameters, as illustrated in Figures 13-16, in addition to the non-uniform parameter (m), the rotation parameter (Ω), the Hartmann number (M), and the phase difference coefficient (ϕ). Figures 13 and 14 illustrate how average pressure rise is affected by the Hartmann number (M) and the phase difference coefficient (ϕ). The findings indicate that average pressure rise decreases with increasing (M) due to the Lorentz force, plus the decreases with increasing (ϕ) and (Ω). Figure 16 illustrates how average pressure rise is affected by increasing the non-uniform parameter (m). The findings indicate that average pressure rise decreases at the top of the canal and increases at its bottom.

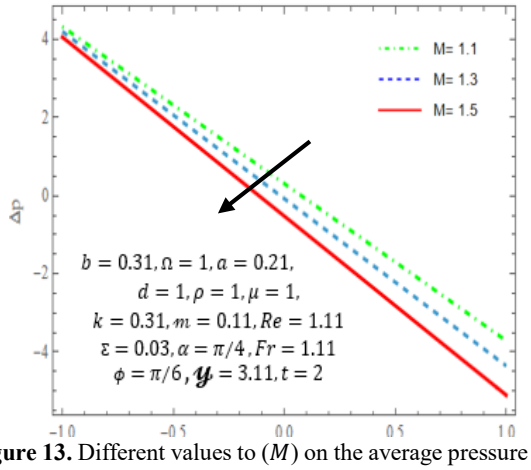

Figure 13. Different values to (M) on the average pressure rise.

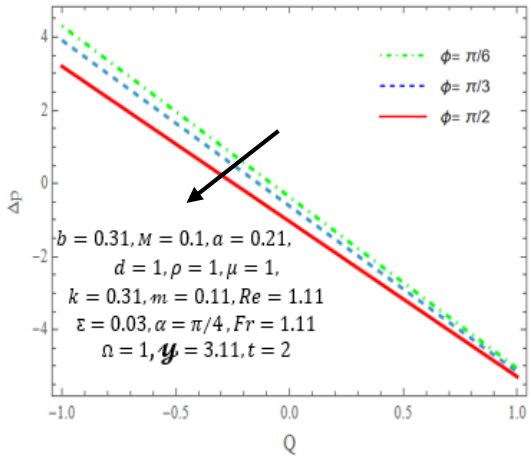

Figure 14. Different values to (ϕ) on the average pressure rise.

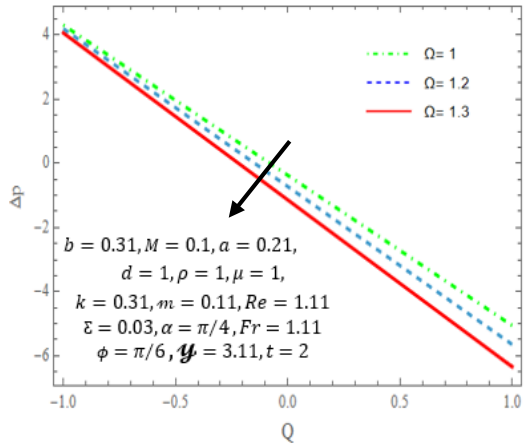

Figure 15. Different values to (Ω) on the average pressure rise.

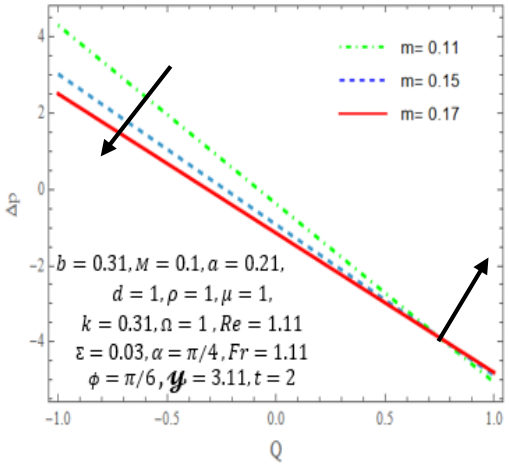

Figure 16. Different values to (m) on the average pressure rise.

5. 4. Temperature Profile

The temperature profile is influenced by various physical parameters, as illustrated in Figures 17-20, in addition to the non-uniform parameter (m), the Prandtl number (Pr), the thermophoresis parameter (Nt), and the phase difference coefficient (ϕ). Figures 17-19 illustrate how temperature profile is affected by the thermophoresis parameter (Nt), the non-uniform parameter (m), and the Prandtl number (Pr). The findings indicate that temperature profile increases with increasing $(Nt), (m), and\ (Pr)$. Figure 20 illustrates how temperature profile is affected by increasing the phase difference coefficient (ϕ). The findings indicate that temperature profile decreases with increasing (ϕ).

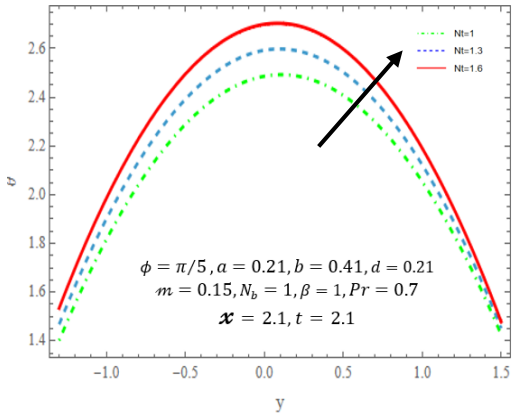

Figure 17. Different values to (Nt) on the temperature profile.

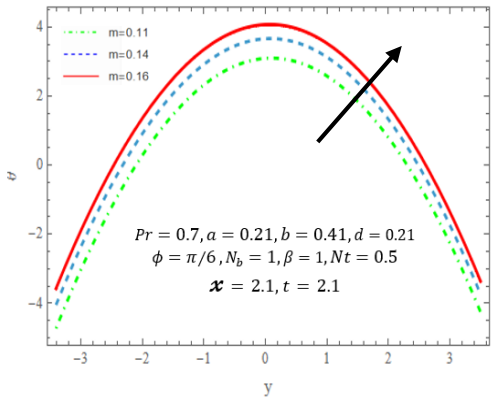

Figure 18. Different values to (m) on the temperature.

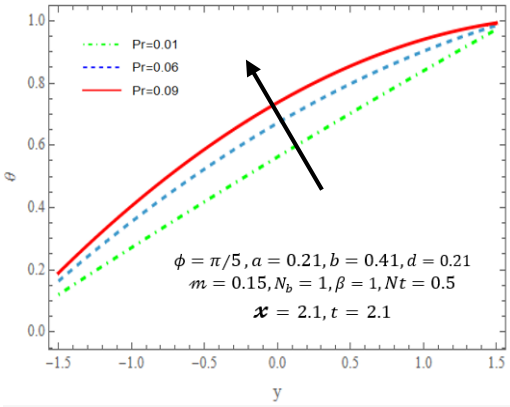

Figure 19. Different values to (Pr) on the temperature profile.

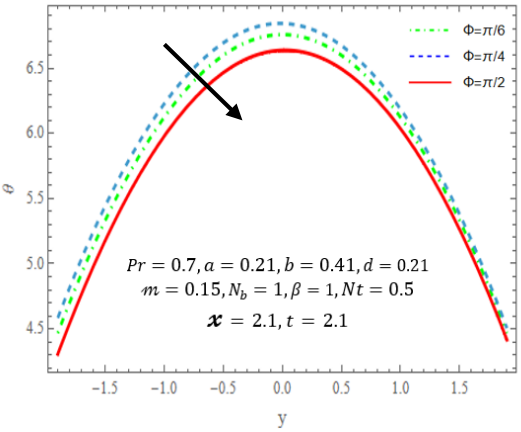

Figure 20. Different values to (ϕ) on the temperature.

5. 5. Nanoparticle Volume Function

The nanoparticle volume function is influenced by various physical parameters, as illustrated in Figures 21-24, in addition to the non-uniform parameter (m), the Prandtl number (Pr), the thermophoresis parameter (Nt), and the phase difference coefficient (ϕ). Figure 21 illustrates how nanoparticle volume function is affected by increasing the thermophoresis parameter (Nt). The findings indicate that nanoparticle volume function increases with increasing (Nt). Figures 22-24 illustrate how nanoparticle volume function is affected by the phase difference coefficient (ϕ), the non-uniform parameter (m), and the Prandtl number (Pr). The findings indicate that nanoparticle volume function decreases with increasing $(\phi), (m)\ and\ (Pr)$.

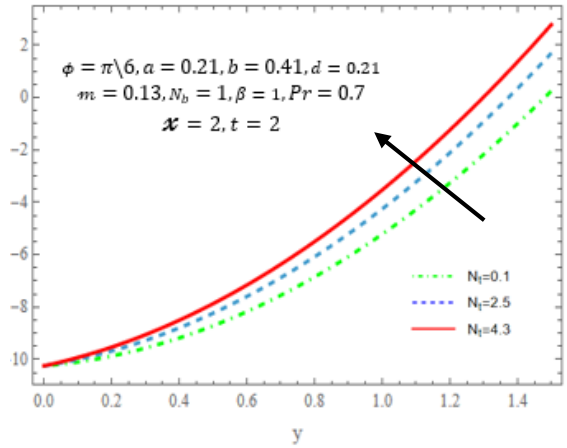

Figure 21. Different values to (Nt) on the nanoparticle volume function.

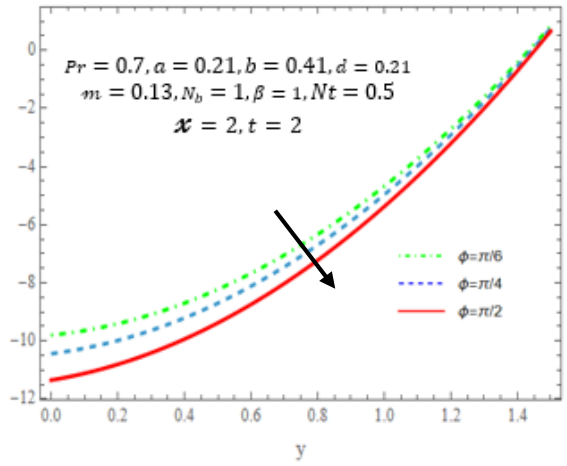

Figure 22. Different values to (ϕ) on the nanoparticle volume function.

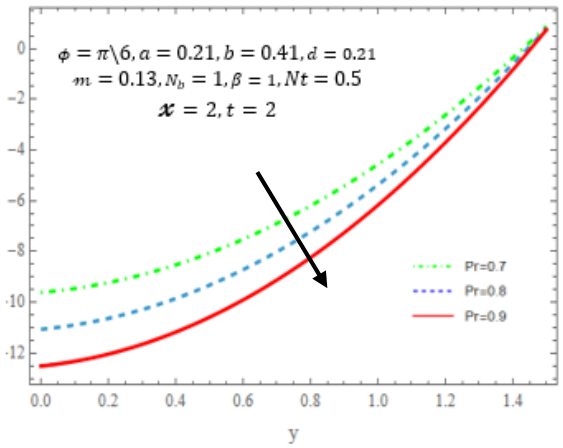

Figure 23. Different values to (Pr) on the nanoparticle volume function.

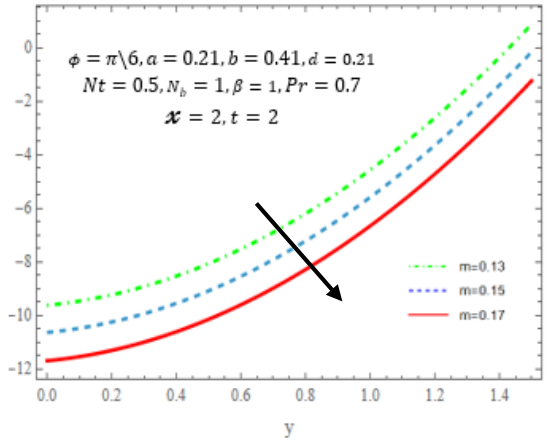

Figure 24. Different values to (m) on the nanoparticle volume function.

6. Conclusion

In this study, a comprehensive mathematical model was developed to examine the peristaltic transport of a pseudoplastic nanofluid in an asymmetric rotating inclined channel under magnetohydrodynamic effects and porous medium resistance.

- The velocity profile increases at the center of the channel and decreases near the walls with increasing Hartmann number M, reflecting the magnetic damping effect and redistribution of momentum due to the Lorentz force. In contrast, the velocity increases in the center channel while decreases to the boundaries with increasing rotation parameter Ω. The velocity profile increases with phase difference(ϕ) rises and decreases as the flow rate (Q) increases.
- The size of the trapped bolus increases with $(Q), (M)$ increases. It is also observed that the volume of the trapped mass decreases as (ϕ) and (m) increases.
- The average pressure rise decreases with increasing (M), (ϕ), and (Ω). The average pressure rise decreases at the top of the canal and increases at its bottom with increasing the non-uniform parameter (m).
- The temperature profile increases with increasing $Nt, m \ and \ Pr$, while it decreases with increasing ϕ.
- The nanoparticle volume fraction increases with increasing Nt, but decreases with increasing $\phi, m, and \ Pr$.

References

Abd-Alla, A., & Abo-Dahab, S. (2016). Rotation effect on peristaltic transport of a Jeffrey fluid in an asymmetric channel with gravity field. *Alexandria Engineering Journal*, *55*(2), 1725-1735.

Ali, H. A. (2021). Radiative peristaltic transport of Ree-Eyring fluid through porous medium in asymmetric channel subjected to combined effect of inclined MHD and convective conditions. *Journal of Physics: Conference Series*, *1879*, 022101.

Ali, H. A., & Salman, M. R. (2024). Influence of rotation on peristaltic flow for pseudoplastic fluid: a wavy channel. *International Journal of Optimization & Control: Theories & Applications*, *14*(4), 336-345.

Choi, S. U. (1995). Enhancing thermal conductivity of fluids with nanoparticles. ASME international mechanical engineering congress and exposition,

Eytan, O., Jaffa, A. J., Har-Toov, J., Dalach, E., & Elad, D. (1999). Dynamics of the intrauterine fluid–wall interface. *Annals of biomedical engineering*, *27*, 372-379.

Hasona, W., Almalki, N. H., ElShekhipy, A., & Ibrahim, M. (2020). Combined effects of variable thermal conductivity and electrical conductivity on peristaltic flow of pseudoplastic nanofluid in an inclined non-uniform asymmetric channel: applications to solar collectors. *Journal of Thermal Science and Engineering Applications*, *12*(2), 021018.

Hayat, T., Farooq, S., Mustafa, M., & Ahmad, B. (2017). Peristaltic transport of Bingham plastic fluid considering magnetic field, Soret and Dufour effects. *Results in physics*, *7*, 2000-2011.

Hayat, T., Iqbal, R., Tanveer, A., & Alsaedi, A. (2016). Influence of convective conditions in radiative peristaltic flow of pseudoplastic nanofluid in a tapered asymmetric channel. *Journal of Magnetism and Magnetic Materials*, *408*, 168-176.

Hayat, T., Noreen, S., Alhothuali, M. S., Asghar, S., & Alhomaidan, A. (2012). Peristaltic flow under the effects of an induced magnetic field and heat and mass transfer. *International Journal of Heat and Mass Transfer*, *55*(1-3), 443-452.

Hina, S., Mustafa, M., Hayat, T., & Alotaibi, N. D. (2015). On peristaltic motion of pseudoplastic fluid in a curved channel with heat/mass transfer and wall properties. *Applied Mathematics and Computation*, *263*, 378-391.

Jaffrin, M., & Shapiro, A. (1969). Discussion:``Peristaltic Transport''. *Journal of Applied Mechanics*, *35*, 669-675.

Latham, T. W. (1966). *Fluid motions in a peristaltic pump* MSc Thesis, Massachusetts Institute of Technology].

Nassief, A. M., & Abdulhadi, A. M. (2023). Rotation and magnetic force effects on peristaltic transport of non-newtonian fluid in a symmetric channel. *Ibn AL-Haitham Journal For Pure and Applied Sciences*, *36*(2), 436-453.

Salman, M. R. (2023). Effect of convective conditions in a radiative peristaltic flow of pseudoplastic nanofluid through a porous medium in a tapered an inclined asymmetric channel. *AIP Conference Proceedings*, *2414*(1), 040026.

Salman, M. R., & Abdulhadi, A. M. (2018). Analysis of heat and mass transfer in a tapered asymmetric channel during peristaltic transport of (pseudoplastic nanofluid) with variable viscosity under the effect of (MHD). *Journal of AL-Qadisiyah for computer science and mathematics*, *10*(3), 80-96.

Salman, M. R., Ali, H. A., Albuohimad, B., & Nasralla, A. M. (2025). Rotation and porous medium impact on MHD peristaltic flow of pseudoplastic fluid through a waveform channel. *Journal of Advanced Research in Fluid Mechanics and Thermal Sciences*, *127*(2), 119-132.

Salman, V. M. R., & Abdulhadi, A. M. (2017). Soret and Dufour effects in MHD peristalsis of pseudoplastic nano fluid with porous medium in tapered channel. *International Journal of Science and Research*, *6*(12), 1939-1951.

Sh Alshareef, T. (2020). Impress of rotation and an inclined MHD on waveform motion of the non-Newtonian fluid through porous canal. *Journal of Physics: Conference Series*, *1591*, 012061.

Shapiro, A. H., Jaffrin, M. Y., & Weinberg, S. L. (1969). Peristaltic pumping with long wavelengths at low Reynolds number. *Journal of fluid mechanics*, *37*(4), 799-825.

Tahir, M., & Ahmad, A. (2020). Impact of pseudoplaticity and dilatancy of fluid on peristaltic flow and heat transfer: Reiner-Philippoff fluid model. *Advances in Mechanical Engineering*, *12*(12), 1-10.

Tripathi, D., & Bég, O. A. (2014). A study on peristaltic flow of nanofluids: Application in drug delivery systems. *International Journal of Heat and Mass Transfer*, *70*, 61-70.